ISTITUTO NAZIONALE DI FISICA NUCLEARE

Sezione di Genova

INFN/FM-97/02
7 Maggio 1997

A. Daccà, G. Gemme, L. Mattera, R. Parodi:

TEMPERATURE INFLUENCE ON THE OXIDATION OF NIOBIUM FOR SUPERCONDUCTING RF CAVITIES

PACS N.: 77.84.Dy, 74.25.Mf, 82.80.Pv

SIS–Pubblicazioni
dei Laboratori Nazionali di Frascati

INFN – Istituto Nazionale di Fisica Nucleare
Sezione di Genova

INFN/FM–97/02
7 Maggio 1997

TEMPERATURE INFLUENCE ON THE OXIDATION OF NIOBIUM FOR SUPERCONDUCTING RF CAVITIES

A.Daccà, G. Gemme, R. Parodi
INFN–Sezione di Genova, Via Dodecaneso 33, I–16146 Genova (Italy)

L. Mattera
Unità INFM–Dipartimento di Fisica, Università degli Studi di Genova, Via Dodecaneso 33, I–16146 Genova (Italy)

Abstract

The surface chemical composition of Nb samples prepared by following procedures commonly employed in the preparation of RF cavities has been studied by XPS and ARXPS.

In order to understand the process occurring at surface, the thermal evolution of the surface has been studied in the 30°C ÷ 1000°C range of temperature both in the heating phase and cooling phase. During the heating phase, an irreversible transition has been observed near T ≅ 200÷300 °C; it is characterized by a progressive reduction of Nb surface oxides from Nb_2O_5 to NbO_2 and finally to NbO. The O signal disappears near T ≅ 1000°C and it reappears below 900°C, during the cooling phase. This can be interpreted as due to O migration in the Nb matrix, raising T, and by O diffusion towards the surface as the temperature decreases.

Work function measurements show that the values of Φ are strongly correlated with the chemical composition of the surface.

1. - INTRODUCTION

Niobium is, at present, the material most widely used in the preparation of superconducting RF cavities for nuclear particle accelerators, even thought, in the last few years, there has been a growing attention to alternative materials, such as NbN and (Nb, Ti)N [1 - 6]. It is then obvious that the studies, started in the sixties, on RF features of niobium, continue now with the support of improved experimental techniques.

The major difficulties about Nb cavities concern the achievement of the critical magnetic field B_C [7 - 9], and the presence of the residual resistance R_{res} that limits RF performances [7 - 9].

The practical use of Nb cavities has shown the existence of a residual resistance, whose value is temperature independent and that strongly affects the quality factor Q. It is well recognized that this resistance is produced by structural imperfections and surface impurities, like O and C, so that a series of surface treatments, both chemical and thermal, have been developed to reduce surface contamination [10].

Results about the oxidation of Nb, either by exposure to air or in a controlled atmosphere of O_2, and the composition of surface layers [11 - 13], and about the consequences of chemical treatments on the surface[14] are well established. On the other hand, an exhaustive and systematic study on the consequences of thermal treatments on Nb is still necessary to understand the major mechanisms operating on the surface during a thermal cycle. In particular, as far as surface oxygen concerns, a group of authors [15, 16] has found that temperatures near 1800°C are necessary to eliminate contamination produced by O, since the evaporation of Nb oxides from the surface begins only above 1600°C, while below these temperatures oxygen atoms tend to migrate into the Nb matrix.

The aim of this study is to investigate the surface properties of Nb, as a result of thermal treatments in the range of temperatures between 30°C and 1000°C. For this reason X-ray photoelectron spectroscopy (XPS) and angle resolved X-ray photoelectron spectroscopy (ARXPS) measurements have been carried out on properly prepared Nb samples, with particular attention to the presence of O and C atoms on the surface.

To obtain further information on RF features of niobium, work function measurements have also been performed, together with the determination of surface chemical composition, in order to correlate the value of the work function with the different compounds present on the surface. The work function, Φ, is a critical parameter, from the point of view of RF properties as, through the Fowler and Nordheim law [17], it controls electron emission from the surface, the typical process occurring inside superconducting cavities.

2. - EXPERIMENTAL

2.1. - X-ray photoelectron spectroscopy

Measurements on niobium samples are performed in a PHI ESCA 5600ci MultiTechnique electron spectrometer. A base pressure of 2×10^{-10} Torr is obtained, in the analysis chamber, by a combination of turbomolecular, ion and titanium sublimation pumps; the residual gas in the analysis chamber is composed of H_2 and H_2O and, to a lower extent, of CO, Ar and CO_2.

Photoelectrons are excited using a standard X-ray source that produces MgKα ($h\nu$ = 1486.6 eV) radiation and a monochromatized source that produces AlKα ($h\nu$ = 1253.6 eV) radiation. The experimental set-up is provided with a SCA (spherical capacitor analyzer) electron energy analyzer, characterized by an energy resolution of 0.5 eV, an ion gun, that produces a beam of Ar ions in the energy range between 2 KeV and 5 KeV, a residual gas analyzer and a fast entry lock for the introduction of the specimen. The specimen mount has four degrees of freedom (X, Y, Z and tilt of ± 50° with respect to the manipulator axis with a resolution of ± 1°) and is provided with an heating filament in tantalum, wrapped on a ceramic mount, that permits to vary the sample temperature between 30°C and 1000°C.

The heating and cooling rates are different according to the different ranges of temperature at which the filament operates. In the heating phase, under 800°C, the heating rate is of the order of ≈ 0.5°C/s, while above 800°C it decreases to ≈ 0.2°C/s; in the cooling phase, the cooling down is produced by conduction from a Cu bar cooled at liquid nitrogen temperature: in this case the rate is of the order of ≈ 0.7°C/s for T > 300÷400°C, and it decreases to ≈ 0.08°C/s under 300°C.

The electron energy analyzer operates in the constant energy mode at a pass energy of 2.95 eV for ARXPS measurements and of 11.75 eV for XPS measurements. The energy scale is calibrated periodically by determining the binding energy of $Au4f_{7/2}$ (84 eV), $Ag3d_{5/2}$ (368.4 eV) and $Cu2p_{3/2}$ (932.6 eV) lines of appropriate samples and by using the spectroscopically pure metals values obtained from Seah [18]. All spectra are recorded by sampling an area of 400 μm/diameter; the acceptance angle is of ± 7° for XPS measurements and of ± 2° for ARXPS measurements. The binding energy values are measured with an accuracy of ± 0.1 eV.

All spectra are taken with the X-ray sources operating at 400 W (15KV - 27mA). The monochromatized X-ray source is located perpendicular to the analyzer axis, while the standard

X-ray source is located at 54.7° with respect to the analyzer axis. In XPS measurements electrons emitted at a take-off angle of 45° are analyzed.

XPS and ARXPS analyses are carried out during thermal cycles in the temperature range between 30 - 1000°C in order to determine the surface chemical composition and the in-depth distribution of the different compounds. In particular, at every fixed temperature we have performed an angular resolved analysis, that allows to evaluate the thickness' of the compounds present on the surface.

Work function values Φ are obtained by measuring the total width of the photoelectron spectrum. Depth profile analysis is performed by alternating XPS spectra and Φ measurements with ion sputtering (Ar^+ at 2 KeV).

2.2. - Sample preparation

We have studied Nb samples obtained from the same plate we use to make RF cavities [19]. This is polycrystalline Nb (linear grain size $\approx$ 2÷4 mm) of 99.95 % purity with 300 ppm of tantalum.

In order to eliminate any possible contribution coming from chemical composition or geometry, we have employed the same specimen (a disk of 20 mm diameter and 5 mm height) to prepare all samples which will be discussed in the present work. All samples were chemically polished first in a 1 : 1 : 1 solution of HNO_3, HF and H_3PO_4. This treatment at T = 18°C for t = 2.5 min removes 20 μm of material [14] so to eliminate from the surface any trace of mechanical machining (or of any previous treatment). After this "basic" treatment, different samples were prepared following procedures commonly employed in the preparation of RF cavities. Each sample is first stored in methyl alcohol and then immediately introduced in the analysis chamber, via the fast entry lock, and exposed to a series of thermal cycles. Once that all measurements are completed, the sample is extracted from the chamber, chemically polished, prepared with a different treatment and introduced again in the chamber for the analysis.

In particular we describe the results obtained on a Nb sample anodized at 5V; anodization of Nb is carried out in a electrochemical cell at T = 27°C, containing a 7 % aqueous solution of ammonia, by applying to the electrodes a d.d.p. of 5V; this treatment results in the growth, on the Nb surface, of a Nb_2O_5 layer, whose thickness depends on the voltage applied to the cell ($\cong$ 0.8÷1 nm/V) [20].

2.3. - Measurements of surface and in-depth composition

Before any thermal treatment we first measure the complete energy distribution of photoelectrons in order to identify the major compound present on the surface. After this identification (essentially Nb and its compound with oxygen and carbon) we analyze the peak shape in order to deconvolute the different components of the spectrum produced by different chemical compounds.

A single line for a conducting material is given by the convolution of the Doniach and Sunjic curve[21] representing the intrinsic shape of the line, with a Gaussian curve which takes into account instrumental effects. The deconvolution of the measured lines is then performed by using asymmetric Gaussian-Lorentzian functions[22]. An example of this procedure is given in Fig. 1, where the Nb3d line has been deconvoluted, after a proper background subtraction, in the Nb3d 5/2 and the Nb3d 3/2 lines.

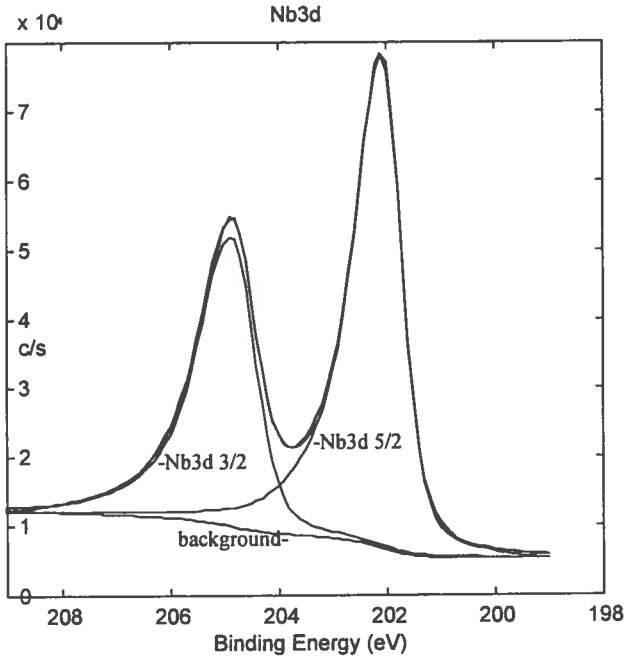

Fig. 1. Deconvolution of the Nb3d line: the lineshape is reproduced by two Gaussian-Lorentzian curves, that represent the Nb doublet, and by the background calculated with the method of Shirley.

To determine the atomic concentration X of the elements present on the Nb surface we used the relation [23]:

$$X_A = \frac{I_A/S_A}{\sum_{i=1}^{N} I/S_i} \qquad (1)$$

where S_A is the sensitivity factor of element A and N is the number of elements present on the surface.

This equation derives from the expression of the intensity of a XPS line *j* at kinetic energy E produced by an element A in an homogeneous sample Z[24]:

$$I_A(j,Z) = T(E)\cdot D(E)\cdot \Sigma \cdot I_0(h\nu)\cdot \Delta\Omega \cdot N_Z \cdot \lambda_Z(E)\cdot \cos\varphi \cdot \frac{d\sigma(j,A)}{d\Omega}\cdot X_A(Z) \qquad (2)$$

where T(E) is the transmission function and D(E) is the detection efficiency of the analyzer; D(E) is a constant for electron energy analyzer that operates at constant pass energy. Σ is the area analyzed, $I_0(h\nu)$ is the X-ray flux at energy hν, ΔΩ is the solid angle of acceptance of the analyzer, N_Z is the atomic density of the sample Z, $\lambda_Z(E)$ is the attenuation length for a photoelectron of energy E in the material Z, $X_A(Z)$ is the atomic concentration of element A in the compound Z, φ is the electron take-off angle relative to the normal to the sample and $d\sigma(j,A)/d\Omega$ is the differential photoelectron cross-section relative to the line *j* of the element A.

As the values of the intensity are always used in ratios in eq. (1), all terms that are constant for a particular geometry (Σ, $I_0(h\nu)$, ΔΩ, cosφ), cancel out and the intensity ratio of two elements A and B can be written as [24]:

$$\frac{I_A}{I_B} = \frac{S_A X_A}{S_B X_B} \qquad (3)$$

where the sensitivity factor S_i is given by:

$$S_i = N_i \cdot \lambda_i(E_i)\cdot \frac{d\sigma(j,i)}{d\Omega}\cdot \frac{1}{E_i} \qquad (4)$$

and the 1/E dependence of S_i is produced by the energy dependence of the transmission function of the analyzer. In this work we use the sensitivity factors of the Handbook of Photoelectron Spectroscopy [25] that are all normalized to the 1s line of fluorine.

The intensity of each XPS line has been evaluated as the area under the peak after a proper background subtraction. The background has been calculated with the Shirley method [26].

To evaluate the in-depth composition, we have performed angle-resolved measurements, by taking advantage of the dependence of the photoelectrons escape depths with take-off angle. At the energy of the incoming photons we use, and being interested in the Nb3d, O1s and C1s lines, the escape depth λ of the photoelectrons is of the order of $3\lambda \leq 60 \div 80$ Å, where the equal sign holds at normal emission.

An angular resolved analysis allows to evaluate film thickness. In the case of an overlayer A on the substrate B, the thickness of the overlayer d_A can be evaluated as[27]:

$$d_A = \lambda_A \operatorname{sen}\theta \cdot \ln\left(\frac{X_A(\theta)}{X_B(\theta)} + 1\right) \tag{5}$$

where $X_A(\theta)$ and $X_B(\theta)$ are the concentrations of species A and B measured at the angle of emission, relative to the surface of the sample, θ. Obviously, eq. (5) can be applied only if $d_A < 3\lambda_{A,B}$ where $\lambda_{A,B}$ are the escape depths of electrons generated from the lines used to detect species A and B, respectively.

At coverages smaller then one monolayer, eq. (5) loses its significance and it has to be replaced by[27]:

$$\Phi_A = \frac{X_A/X_B}{1 + X_A/X_B} \cdot \frac{1}{1 - \exp\left(-\frac{a_A}{\lambda_A \operatorname{sen}\theta}\right)} \tag{6}$$

where Φ_A is the fractional coverage and a_A is the atomic dimension of the species A.

Eqs. (5-6) were written in the hypothesis that species A and B are two different compounds of the same element so that a single attenuation length can be introduced.

The values of the attenuation length have been calculated by using the expressions of Seah and Dench [28]:

for elements

$$\lambda = \frac{538}{E^2} + 0.41\sqrt{aE} \quad \text{nm} \tag{7}$$

for oxides

$$\lambda = \frac{2170}{E^2} + 0.55\sqrt{aE} \quad \text{nm} \tag{8}$$

for inorganic compounds

$$\lambda = \frac{2170}{E^2} + 0.72\sqrt{aE} \quad \text{nm} \tag{9}$$

where E, in eV, is the kinetic energy relative to XPS line of the element considered and a, in nm, is the dimension of the atom or compound. The values of λ used in this work are reported in Table I.

Table I. Attenuation length values (λ) calculated with Eqs. 7 - 9; in the first column in parenthesis there is the XPS line considered for the evaluation of λ. In the second column there is the dimension of the atom or of the compound, in the third the kinetic energy corresponding to the XPS line considered and in the last column the λ values.

Compound	**a (nm)**	**E (eV)**	**λ (nm)**
Nb (Nb3d)	0.32	1281	2.5
NbO (Nb3d)	0.33	1270	3.7
NbO_2 (Nb3d)	0.33	1277.2	3.7
Nb_2O_5 (Nb3d)	0.45	1275.7	5.8
NbC (C1s)	0.33	1201.2	4.7
Grafite (C1s)	0.35	1199.2	2.9

3. - RESULTS AND DISCUSSION

3.1. - General aspects

Results concerning XPS measurements performed on Nb anodized at 5V are summarized in Fig. 2. In Fig. 2.a the dependence, during the heating process, of the surface concentration of niobium, oxygen and carbon on temperature is represented. A first change at T ≅ 280÷380°C may be observed: it is characterized by a sharp decrease of the concentrations of C and O and by a remarkable increase of the Nb concentration; for T above 700°C the C1s signal disappears, while at T = 1000°C the surface is devoid of contaminants, with a very weak signal of the O1s line.

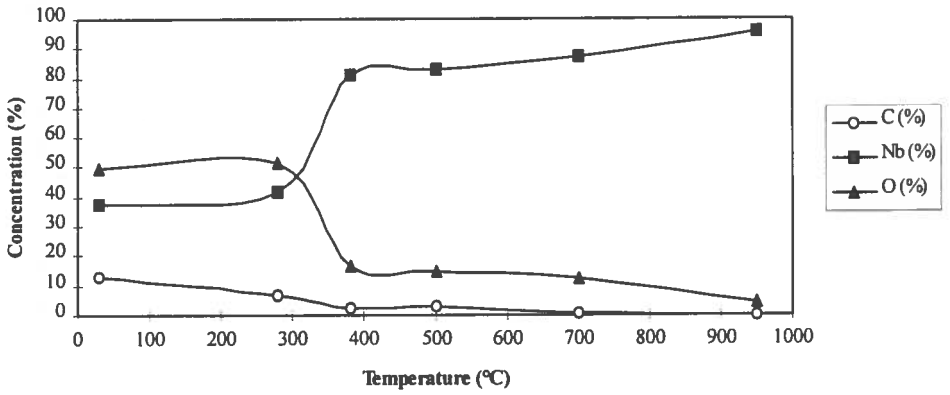

Fig. 2.a. Nb, O and C surface concentration vs increasing temperature, for Nb anodized at 5V.

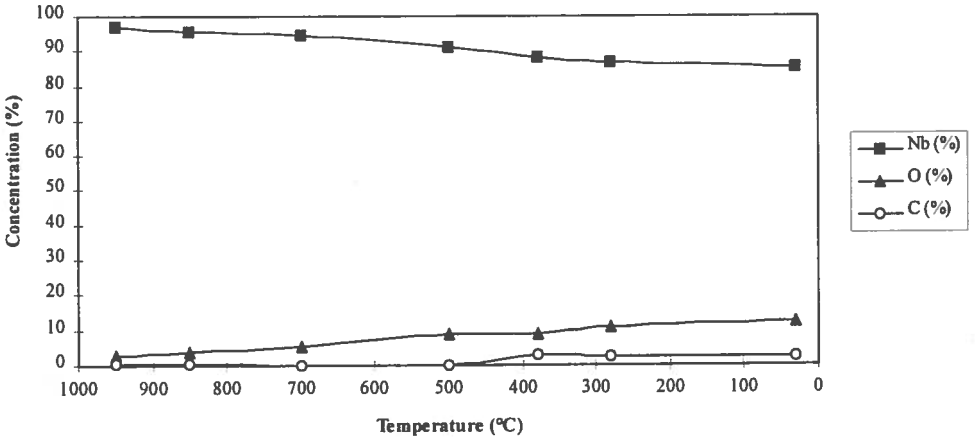

Fig. 2. b. Nb, O and C surface concentration vs decreasing temperature, for Nb anodized at 5V.

During the cooling down phase (Fig. 2.b), the growth of the O1s signal is detectable starting from temperatures around 900÷700°C; on the other hand, the presence of C atoms on the surface is noticed only for T < 500°C and the increase of the C1s signal is much smaller than the one of the O1s signal.

3.2. - The transition Nb_2O_5 - NbO

At room temperature, before any thermal treatments, the XPS and ARXPS measurements give the following surface composition: a layer of Nb oxide, in form of Nb_2O_5, about 60 Å thick (≅ 15 monolayers), upon which there is a layer of C, in graphitic form, whose thickness is of a few monolayers. The thickness of the Nb_2O_5 layer is consistent with that expected for an anodization of the sample at 5V.

In the range of temperature between 200°C and 380°C the sample reveals a surface transition, consisting in the disappearance of the Nb3d doublet, typical of Nb_2O_5, and the corresponding appearance of the Nb3d line at E_B = 202.3 eV, representing pure Nb [25] (Fig. 3). At the same temperatures it may be noticed the disappearance of the C1s line at E_B = 284.5 eV, produced by graphite, and the presence of a line at E_B = 281.8 eV, generated by niobium carbide [25] (Fig. 4). Furthermore the O1s line is characterized by a remarkable decrease of intensity (Fig. 5).

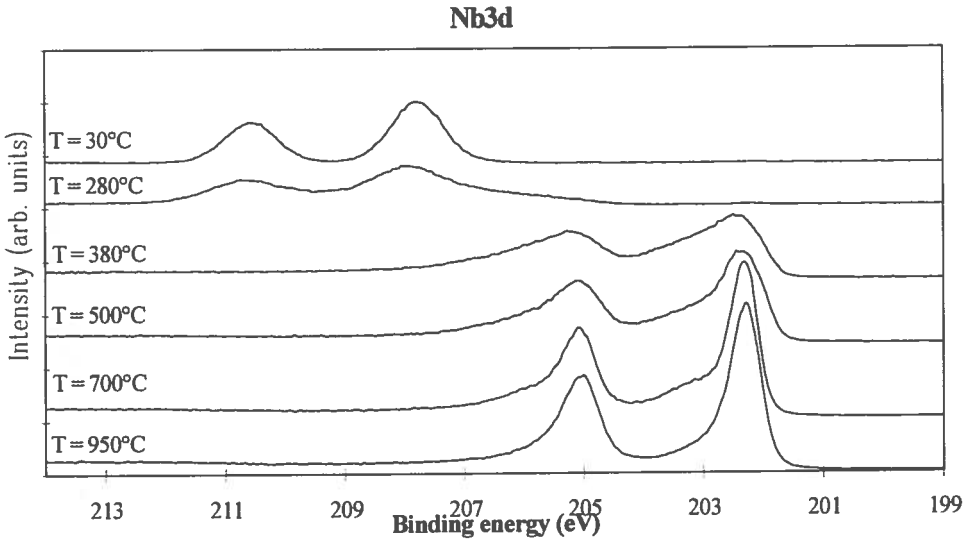

Fig. 3. Evolution of Nb3d line during the heating phase, relative to sample anodized at 5V.

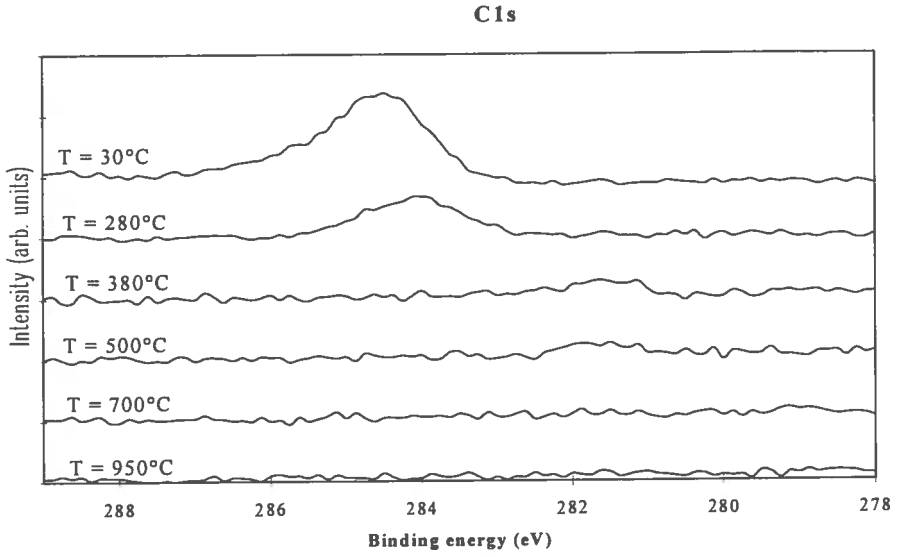

Fig. 4. Evolution of C1s line, during the heating phase, relative to sample anodized at 5V.

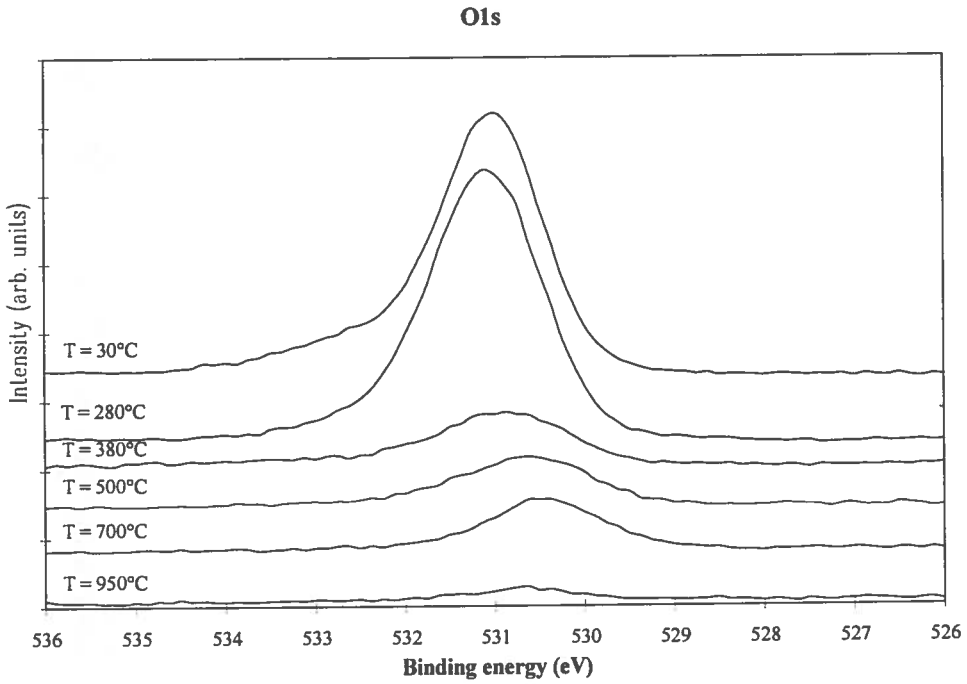

Fig. 5. Evolution of O1s line, during the heating phase, relative to sample anodized at 5V.

ARXPS analysis, performed both during the heating and cooling phases, gives the in-depth composition of Nb oxides summarized in Fig. 6.a and in Fig. 6.b., respectively. The thickness of

the different oxides present on the Nb surface have been calculated using Eqs. (5) and (6) and the analogous ones for multilayers, after a careful decomposition of the Nb3d line shape.

During the heating cycle, the thickness of the Nb_2O_5 layer decreases (Fig. 6.a). At T = 200°C, under the Nb_2O_5 layer, another Nb oxide appears, NbO_2 (identified by the value of binding energy, E_B = 206.1 eV): this compound is detectable only in the range between 200°C and 350°C. When T raises from 350°C to 500°C, NbO appears (E_B = 203.2 eV), and upon 500°C this is the only compound which is detected with a decreasing thickness.

The in-depth composition of Nb oxides shows a less complex behaviour during the cooling down process (Fig. 6.b), in fact only a layer of NbO is detectable on Nb surface, with a thickness that increases, diminishing T, but that never reaches the starting thickness of Nb_2O_5, at room temperature.

The observed transition, that involves a progressive reduction in the oxidation number of Nb (that changes from Nb_2O_5 to NbO_2 and finally to NbO), takes place together with a change in the chemical state of carbon: this element passes from the graphitic form to a bonding state with Nb (NbC) and during this transformation there is a sharp decrease of the C layer thickness (Fig. 7.a).

The same measurements, performed on other Nb samples obtained with different surface treatments (such as chemical polishing, exposition to air or anodization at different voltages), show the same qualitative behaviour; the principal difference consists in the temperature at which the various transitions take place. In particular the temperature, for the transition Nb_2O_5 - NbO, increases with the increasing thickness of the starting layer of Nb_2O_5: it is 200°C for a sample exposed to air, with about 10 monolayers of Nb_2O_5 at room temperature, and grows till 380°C for a sample anodized at 20V, on which there are about 60 monolayers of Nb_2O_5 at room temperature. The described transition is clearly irreversible, because decreasing T, after the reduction from Nb_2O_5 to NbO has occurred, we do not observe again the presence of Nb_2O_5 layer on the surface, but only of a NbO layer.

The transition is probably produced by a desorption process. O atoms coming from Nb_2O_5, combine with C atoms, present on top of the Nb_2O_5 layer as graphite, and leave the surface as CO and, most probably, as CO_2. In fact the process cannot be caused only by a migration to the bulk of surface oxides, because in this case there should be, under the Nb_2O_5 layer, a NbO_2 layer 25÷ 30 monolayers thick (and not 10 monolayers thick, Fig. 6.a), which is not revealed by the ARXPS analysis. Also the assumption of a migration of oxygen from the surface to the bulk matrix is improbable, since the mobility of oxygen in niobium is low for T < 700°C [29] and,

furthermore, this process would not explain the contemporary decrease in the signal of the C1s line.

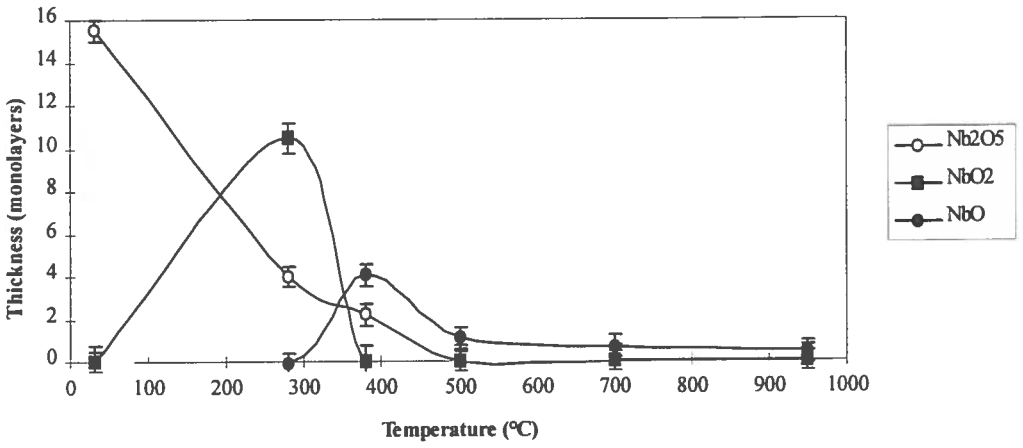

Fig. 6.a. Thickness of Nb_2O_5, NbO_2 and NbO layers on Nb surface vs increasing temperature.

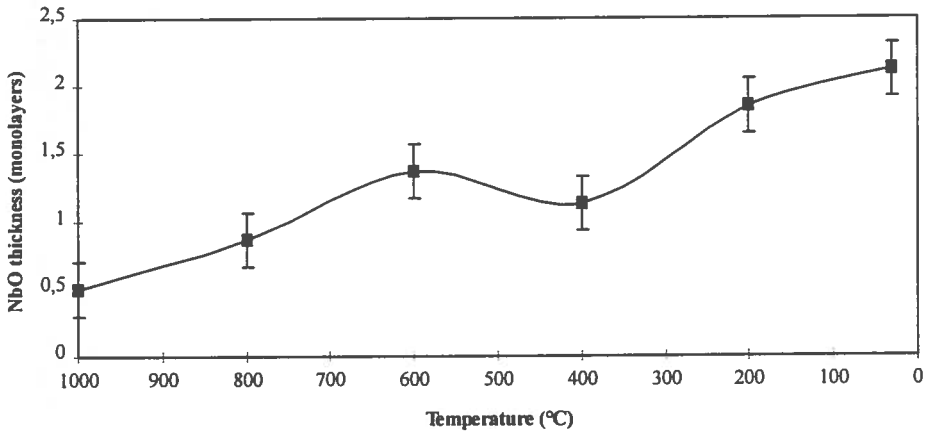

Fig. 6.b. Thickness of NbO layer on Nb surface vs decreasing temperature.

3.3. - Evolution of O concentration

The evolution of the surface concentration of oxygen and the changes of the thickness of Nb oxides as a consequence of thermal treatments are summarized in Figs. 2 and 6.

During the heating phase, in addition to the transition near 200 ÷ 300°C, a further decrease in O concentration (as NbO) may be observed, with the consequent disappearance of the signal at T = 1000°C.

In the cooling phase there is an increase in the intensity of the O1s signal already at T = 900°C, corresponding to the formation of a NbO layer, whose thickness raises decreasing T.

The disappearance of the O1s signal occurs at different temperatures for the different samples (in the range between 30°C and 1000°C), but, for every single sample, this temperature coincides with that at which the O1s line reappears during the cooling down. The formation and the growth of a NbO layer, diminishing T, show different rates and increments for the various samples, which depend strictly on the initial state.

In fact, the NbO layer present on Nb surface at room temperature at the end of a thermal cycle has a thickness roughly proportional to the concentration of oxygen measured on the surface before the beginning of the thermal cycles.

From these experimental results it emerges that this NbO layer is mainly produced by oxygen migration from the bulk towards the surface. Adsorption of oxygen from residual gas background (CO, CO_2, H_2O) can only play a minor role as the background pressure is always the same and does not depend on the sample under study and some samples show a growth of NbO layer characterized by a growth rate too fast to be explained only by a surface contamination from the residual gas.

Since the measurements performed decreasing T show the presence of a source of oxygen inside the sample, the decrease and the disappearance of the O1s signal for T > 700°C can be explained partly with a desorption process from the surface and partly with a diffusion process of O2, towards the bulk of the sample. This assumption is in agreement with the fact that above 700°C all the samples present no more traces of C1s signal and, therefore, surface O atoms cannot combine with it and come out as CO or CO_2. Moreover from T ≅ 700÷800°C onwards the mobility of oxygen in Nb is high and therefore it is possible that O atoms, in form of O_2, dissolves into the Nb matrix[16].

Studies performed previously [30] show that near 1600÷1800°C the oxygen amount produced by the reactions:

$$NbO \leftrightarrow Nb + \tfrac{1}{2} O_2$$

$$NbO_2 \leftrightarrow Nb + O_2$$

is negligible.

As ARXPS analyses do not allow to reveal the presence of an NbO layer subsurface, this means that, above 700°C, O atoms migrate into the bulk of the sample, for a length superior to

the penetration depth of the spectrometer (that is the escape depth of photoelectrons ≈ 20 monolayers). At T = 1000°C the intensity of the O1s line becomes comparable with the noise signal.

3.4. - Evolution of C concentration

The evolution of C concentration during the thermal cycles is represented in Fig. 2, while the changes in the thickness of the carbon layer are summarized in Figs. 7.a and 7.b.

Using the ARXPS analysis, it is possible to establish that the layer of carbon is on the top of the Nb oxides and to determine its thickness during the thermal treatments.

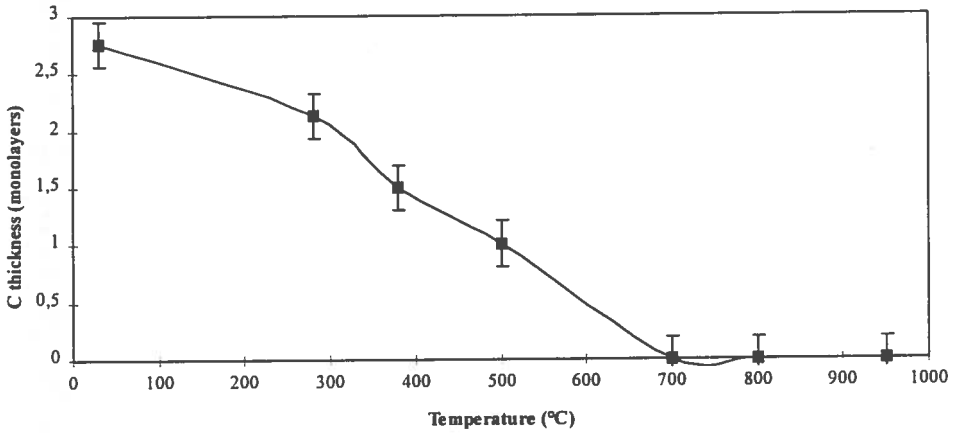

Fig. 7.a. Thickness of C layer on Nb surface vs increasing temperature.

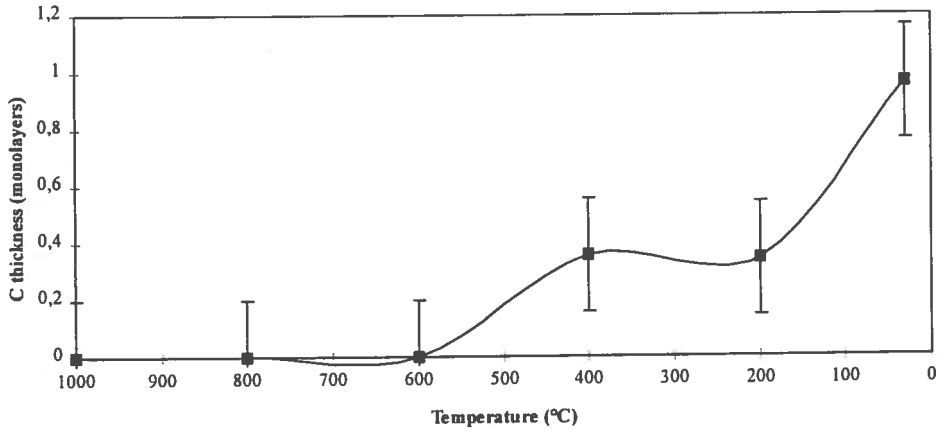

Figs. 7.b. Thickness of C layer on Nb surface vs decreasing temperature.

In the heating phase, the thickness of C layer (initially around 2÷3 monolayers) diminishes and this element is no more detectable above 700°C; decreasing T, the C1s signal reappears below 500÷400°C, with a very reduced thickness, that reaches one monolayer only at room temperature.

The major constituent of the C1s line at room temperature is the graphite signal (E_B = 284.5 eV[25], Fig. 4), while the NbC signal (E_B = 281.8 eV) is present only for T > 200°C and with a smaller intensity with respect to the graphitic one. During the cooling phase, the C1s signal appears for T < 500°C, as NbC, and only at room temperature the signal at E_B = 284.5 eV, produced by graphite, is detectable.

The spectra obtained by ARXPS measurements do not allow to carry out the decomposition of the line shape, in order to resolve the NbC signal from the graphite one, since they do not show considerable changes in the intensities with the variation of the photoelectron take-off angle and, in any case, the C layer has a too small thickness (always inferior to 3 monolayers).

These results underline that the variations of the C1s line, during the thermal cycles, are less correlated to the temperature of the sample, unlike the O1s line.

The fact that the surface concentration of carbon vanishes above 700°C is explained by the desorption process, in which C atoms combine with O atoms and they leave the Nb surface as CO and CO_2.

The formation of a C layer under 500°C (whose thickness reaches one monolayer at room temperature) occurs in times that do not allow to exclude contamination from residual gas, since this process shows features which are independent of the sample analyzed. The amount of carbon present on the surface at the end of one thermal cycle is completely consistent with that (≈ 2÷3 %) revealed on a Nb sample in consequence of the contamination produced on the surface by the residual gas of the analysis chamber (CO, CO_2).

To quantify this type of contamination, an XPS measurement of the C1s and of the O1s lines has been performed on a surface free of contaminants (obtained with Ar^+ sputtering); during this measurement (that lasts about 70 minutes) the only source of contaminants, except the residual gas, was the filament of the X-ray source. This analysis has been performed with an electron take-off angle of 45°, at room temperature and with a base pressure in the analysis chamber of 2 x 10^{-10} Torr; the results are summarized in Fig. 8. We can then conclude that the increase of the C1s signal during the cooling down can be ascribed to the contamination by the

residual gas and it occurs first with the formation of a NbC layer and, subsequently, with the growth of a graphite layer.

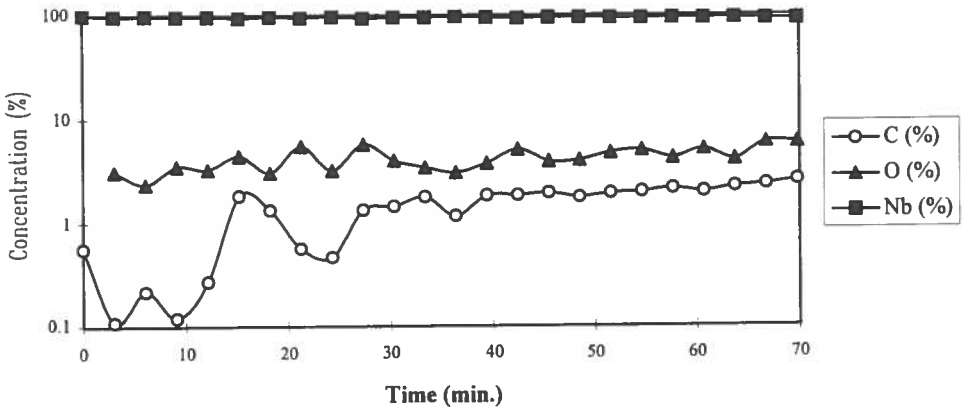

Fig. 8. Contamination produced on Nb sample by the residual gas of the analysis chamber (data are reported on logarithmic scale).

3.5. - Work function

Work function measurements are performed on a sample anodized at 20V, measuring the total width of the photoelectron spectrum. The correlation between Φ values and the in-depth composition is obtained alternating the acquisition of the XPS spectra with ion sputtering.

The evolution of Φ values with the analyzed depth (Fig. 9) can be compared with the chemical composition of the Nb surface (Fig. 10). The surface anodized and introduced in the spectrometer shows a low value of Φ ($\Phi \cong 3.8$ eV), corresponding to the presence of a 20% of carbon on the surface. After the first minutes of sputtering, the C1s signal disappears from the surface and Φ reaches its maximum value of 5.2 eV; carrying on with sputtering, Φ decreases and reaches, in correspondence of the clean surface, the value of 4.2 eV, that is exactly the Φ value of pure Nb.

It may be noticed that there is a clear dependence of Φ on chemical surface composition: the main changes in Φ are all correlated with the changes in the surface concentrations of niobium, oxygen and carbon.

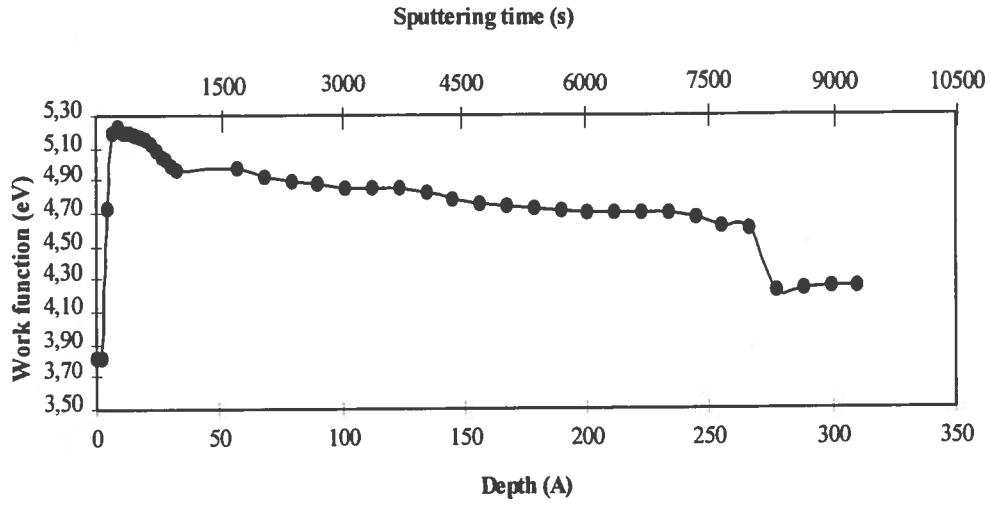

Fig. 9. Nb work function vs depth, relative to Nb anodized at 20 V.

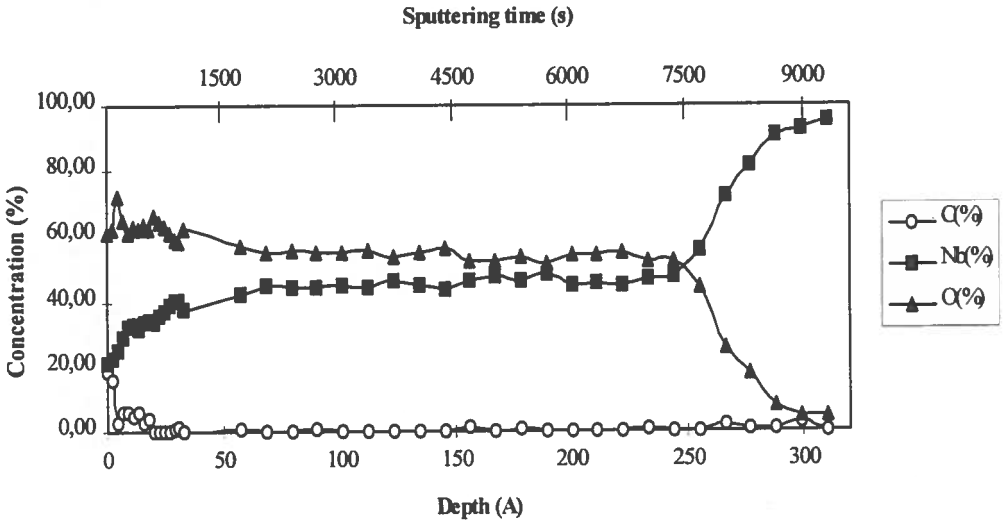

Fig. 10. Nb, O and C concentration vs depth, relative to Nb anodized at 20 V.

Therefore the presence of contaminants, such as carbon, produces a remarkable decrease of Φ, while the presence of oxygen on the surface increases the work function; this is caused by the high electronegativity of oxygen, that produces an increase of the potential barrier, generated by surface dipoles, responsible for the value of Φ.

4. - CONCLUSIONS

The processes observed on Nb surface during the thermal cycles and for different chemical surface compositions are:

1) in the range of T between 200 and 380°C, the reduction of surface Nb oxides from Nb_2O_5 to NbO: the Nb_2O_5 layer becomes poor of oxygen, that partly combines with carbon and leaves the surface as CO and CO_2 and, to a lower extent, migrates as O_2 into the Nb matrix (the mobility of oxygen in Nb at those temperature is low);
2) above 700°C, the intensity of the O1s signal decreases and this is caused both by a desorption process of oxygen from the surface and by the oxygen migration in the bulk. We can exclude the desorption of NbO since NbO has a very high cohesive energy and it sublimates only near 1600÷1800°C[15,16]. These processes justify the increase of the O1s signal during the cooling phase, that shows different dynamic features in the various sample and that cannot be caused only by contamination produced by the residual gas;
3) above 700°C the C1s signal is no more detectable and the formation of a C layer, during the cooling down, for T < 500°C is completely consistent with a contamination process caused by the residual gas; this growth of a carbon layer occurs first with the formation of an NbC layer and, then, at room temperature, with a graphitic layer;
4) the values of the Nb work function are strictly correlated with the chemical composition of the surface. In particular, there is a decrease of 0.4 eV, with respect to the Φ value of metallic Nb, with a C layer on the Nb surface. A Nb_2O_5 layer produces instead an increase of about 1 eV compared to the Φ value of 4.2 eV, typical of pure Nb.

XPS and ARXPS measurements have also been performed on other samples different from the Nb sample anodized at 5V, to which the previous discussion refers. These samples were prepared following procedures commonly employed in standard RF cavities preparations. The results obtained underline that the surface evolution during the thermal cycles is qualitatively the same, independently from the specific surface treatment. The principal difference concerns the temperatures at which we observe the surface transitions: they increase with the increasing thickness of the surface layer of Nb_2O_5. Moreover the growth of O1s signal during the cooling phase show different dynamic features for the various samples, while the pressure conditions and the cooling times are the same; this fact permits to conclude that the NbO layer present on Nb surface after a thermal treatment cannot be produced only by adsorption of the residual gas of the analysis chamber.

REFERENCES

(1) J. R. Gavaler, D. W Deis, J. K. Hulm, C. K. Jones, Appl. Phys. Lett. 15, 10 (1969).

(2) S. Isagawa, J. Appl. Phys. 52 , 921 (1981).

(3) P. Fabbricatore, P. Fernandes, G. C. Gualco, F. Merlo, R. Musenich, R. Parodi, J. Appl. Phys. 66 , 12 (1989).

(4) R. Di Leo, A. Nigro, G. Nobile, R. Vaglio, J. Low Temp. Phys., 78 Nos. ½ (1990).

(5) C. Benvenuti, P. Chiggiato, L. Parrini, R. Russo, Nucl. Instr. Meth. Phys. Res. A336 , 16 (1993).

(6) P. Fabbricatore, G. Gemme, R. Musenich, R. Parodi, M. Viviani, B. Zhang, V. Buscaglia, IEEE Trans. Appl. Supercon., 3, n° 1, 1761 (1993).

(7) H. Piel, CAS Proc., CERN 89-04, (1989).

(8) W. Weiengarten, CERN / AT - RT (int) 92-3, (1992).

(9) J. Halbritter, Proc. Workshop on RF Superconductivity, KfK 3019 ,190, (1980).

(10) P. Kneisel, Proc. Workshop on RF Superconductivity, KfK 3019, 27 (1980).

(11) M. Grunder, J. Halbritter, J. Appl. Phys., 51 (1), 397, (1980).

(12) M. Grunder, J. Halbritter, Surf. Sci. 136 , 144, (1984).

(13) J. Halbritter, Kernforschungszentrum Karlsruhe GmbH, Primarbericht, 08-02-02 P10A

(14) K. Asano et al., KEK Report 88-2, (1988).

(15) H. H. Farrell, H. S. Isaac, M. Strongin, Surf. Sci., 38 , 31 (1973).

(16) M. Strongin, H. H. Farrell, H. J. Halama, O. F. Kammerer, C. Varmazis, Partic. Accel., 3 , 209 (1972).

(17) R. H. Fowler, L. Nordheim, Proc. Royal Society, 119, 173 (1928).

(18) M. P. Seah, Surf. Interface Anal., 14, 488 (1989).

(19) P. Fabbricatore, G. Gemme, R. Musenich, R. Parodi, S. Pittaluga, Proc. 7th Workshop on RF Superconductivity, 385 (Gif sur Yvette, 1995).

(20) T. Imamura, S. Hasuo, IEEE Trans. Appl. Superconduct., vol. 2, 84 (1992).

(21) S. Doniach, M. Sunjic, J. Phys. C Solid State Phys., 3, 285 (1970).

(22) R. I. Jenrich, P. F. Sampson, Technometrics, 10, n° 1 (1968).

(23) L. E. Davis, N. C. MacDonald, P. W. Palmberg, G.E. Riach, R. E. Weber, "Handboook of Auger Electron Spectroscopy" 2nd ed., Phisical Electronics Industries Inc., Minnesota (1976).

(24) D. Briggs, M. P. Seah, "Practical surface analysis by Auger and X-ray photoelectron spectroscopy", Wiley, New York (1983).

(25) J. F. Moulder, W. F. Stickle, P. E. Sobol, K. D. Bomben, "Handbook of X-Ray Photoelectron Spectroscopy", Perkin-Elmer Corporation, USA (1992).

(26) D. A. Shirley, Phys. Rev. B, 5, 4709 (1972).

(27) C. S. Fadley, Prog. Surf. Sci., 16, 3 (1984).

(28) M. P. Seah, W. A. Dench, Surf. Interface Anal., 1, 2 (1979).

(29) R. A. Pasternak, U. S. AEC Interim Report TID - 19489, 11 (1963).

(30) L. H. Rovner, D. Drowart et al., Thecnical Report AFML - 68 - 200, Air Force Material Laboratory, Wright - Patterson Air Force Base, Dayton, Ohio.